INTERNATIONAL JOURNAL FOR NUMERICAL AND ANALYTICAL METHODS IN GEOMECHANICS
Int. J. Numer. Anal. Meth. Geomech. 2000; **00**:1–6 *Prepared using* nagauth.cls *[Version: 2002/09/18 v1.02]*

A new approach for modelling slip lines in geological materials with cohesive models

Rabczuk T.*, Areias P.M.A.

Department of Mechanical Engineering, Northwestern University
Evanston, IL 60208-311, U.S.A
e-mail: t-rabczuk@northwestern.edu

SUMMARY

A methodology to model slip lines as strong displacement discontinuities within a continuum mechanics context is presented. The loss of hyperbolicity of the IBVP is used as the criterion for switching from a classical continuum description of the constitutive behavior to a traction-separation model acting at the discontinuity surface. A version of the element free Galerkin (EFG) method is employed where the slip line is represented as a set of slipped particles. The representation of the slip line as set of cohesive segments promises to remove difficulties in the propagation of the slip line. Two dimensional examples are studied using the Drucker-Prager material model. Copyright © 2000 John Wiley & Sons, Ltd.

KEY WORDS: *meshfree methods, slip line; loss of hyperbolicity; traction-separation laws*; LaTeX 2_ε; class file

1. INTRODUCTION

A slip line can be described as a narrow region in a solid undergoing intense shearing. Slip lines are material instabilities whose kinematical description is similar to mode II fracture. We will exploit this similarity in our approach.

One of the first approaches that treated cracks and slip lines as discontinuity in the displacement field are embedded discontinuity models (Belytschko et al. [7], Armero and Garikipati [4], Oliver et al. [21]). In these models, generally no representation of the slip line is necessary. However, it is well known that without enforcing crack path continuity, the numerically computed results show a mesh bias. Hence, a globally continuous slip plane would have to be used resulting in the necessity of a representation of the set of discontinuous displacements.

*Correspondence to: Department of Mechanical Engineering, Northwestern University
Evanston, IL 60208-311, U.S.A

Contract/grant sponsor: Publishing Arts Research Council; contract/grant number: 98–1846389

Received
Revised

Another very popular class of methods for modelling problems with discontinuities are interelement separation models, see Xu and Needleman [33], Camacho and Ortiz [12], Ortiz et al. [22], Zhou and Molinari [35]. They were originally developed for cracks and later extended to shear bands, Yang et al. [34]. In these methods, cracks, shear bands and slip lines are only allowed to develop along existing interelement edges. This provides the method with comparative simplicity, but can result in an overestimate of the dissipated energy when the actual discontinuity paths are not coincident with element edges. Mesh sensitivity has been reported, see Falk et al. [15]; this sensitivity can be mollified by adding randomness to the strength, as in Zhou and Molinari [35], though such corrections are not yet completely understood.

The extended finite element method is a method that allows the crack or slip line to propagate arbitrarily. Methods for static crack problems in two and three dimensions were developed by Moes and Belytschko [19], Moes et al. [20] and Gravouil et al. [16], respectively. The method was applied to dynamic crack problems in Belytschko et al. [6] and to dislocations in Ventura et al. [32]. A recent paper applies the extended finite element method to discontinuous modelling of shear bands in metals, Areias and Belytschko [3], Samaniego and Belytschko [28]. However, these methods require an explicit representation of the crack or shear band surface, which usually has been provided by level sets. This makes the treatment of phenomena such as branching and multiple cracking more difficult, since another level set needs to be introduced whenever a branch occurs. Also criteria that determine crack branching are questionable.

The proposed method is motivated by the *cracking* particle technique, Rabczuk and Belytschko [23, 25], that was used for modelling cracks in mode I and mixed mode failure problems. A major advantage of this particle method, or of particle methods in general, is that even without enforcing crack path continuity, mesh independent results are obtained; no mesh alignment sensitivity occurs. In this paper, we will modify this approach for pure mode II failure that occurs in shear bands, e.g in metals, and in slip lines, e.g. in geological materials such as rock or soil. Though the failure mode in metallic shear bands is the same, we believe that there is a major difference when applying this technique to slip lines in geological materials. First, in geological materials, a *real* discontinuity occurs in contrast to shear band where the material is glued up to extremely large deformation states when the material separates. Second, shear bands in metals usually occur under dynamic loading where strain rate and temperature effects play an important role whereas in many geological applications such effects can be neglected. The latter issue is important since for viscous constitutive models the problem is no longer ill-posed, hence elipticity or hyperbolicity, in the dynamic, will not be lost.

Within this paper, the transition to *sheared* particles is governed by loss of hyperbolicity. After hyperbolicity is lost, a discontinuity in the displacement field is introduced. This is accomplished by enriching the test and trial function with additional unkowns that will determine the jump in the discplacement field. The major difference to the approach in [23] is, that only displacement jumps parallel to the slip line are allowed. This is accomplished by introducing instead of two additional unknowns, only one additional unknown into the variational formulation; in the two dimensional case, that acts in the direction of the shear band line. This way, only one-dimensional cohesive models become necessary; in the 2D case.

The wording "particle" method might be misleading within the context of geomechanics. We would like to clarify that we don't actually model rigid or elastic particles that can contact each other and transmit forces. Instead, our approach is continuum based. But instead of using

finite elements, we use a meshfree method, sometimes also called particle method.

We would like to mention that our intention is not to develop models to exactly predict slip lines in geological materials but to show the applicability of our method. Hence, we have chosen a rather simple constitutive model (Drucker-Prager) though more complex models can be used.

The paper is organized as follows. First, the use of the local hyperbolicity of the momentum equation as a criterion of material stability is motivated. Then, the problem of a solid with a dissipative interface is formulated. The constitutive equations for the bulk material and the dissipative interface are also discussed. We end the paper with three examples that show the ability of the method to capture slip lines in geological materials.

2. SLIP LINE ONSET

A shear band in a rate-independent material results from a material instability. A classical definition of material stability is based on the so-called Legendre-Hadamard condition, which establishes that for any non zero vectors $\mathbf{n}$ and $\mathbf{h}$ the following point-wise inequality must hold:

$$(\mathbf{n} \otimes \mathbf{h}) : \mathbf{A} : (\mathbf{n} \otimes \mathbf{h}) > 0 \tag{1}$$

where $\mathbf{A}$ is the constitutive tangent operator. For a linear comparison solid, if non-propagating singular surfaces do not occur, the Legendre-Hadamard condition is identical to the strong-ellipticity condition, used e.g. in Simo et al. [30]. In case, eq. (1) is no longer fullfilled, the material looses stability and $\mathbf{n}$ defines the direction of propagation, and $\mathbf{h}$ is the *polarization* of the wave. This condition ensures that the speed of propagating waves in a solid remains real. Equality in expression (1) is the necessary condition for stationary waves. Belytschko et al. [9] give a textbook description for obtaining condition (1) by means of a stability analysis of the momentum equation when a perturbation of the form $\boldsymbol{u} = \boldsymbol{h} \exp(i\omega t + k\boldsymbol{n} \cdot \boldsymbol{x})$ is applied. The Legendre-Hadamard condition is ocasionally called strong ellipticity of the constitutive relation (see Marsden and Hughes [18]). In the dynamical case, the Legendre-Hadamard condition implies the hyperbolicity of the IBVP. The reader is referred to Silhavy [29] for details about the concepts mentioned above.

Based on expression in (1), let us define for a given material point of a solid at a given time,

$$\mathbf{Q} = \mathbf{n} \cdot \mathbf{A} \cdot \mathbf{n} \tag{2}$$

where $\mathbf{Q}$ is the acoustic tensor with components $Q_{ik} = n_j n_l A_{ijkl}$. We say that a material point is stable whenever the minimum eigenvalue of $\mathbf{Q}$ is strictly positive, and unstable otherwise.

One difficulty is that the analysis of the acoustic tensor generally will give us two directions $\mathbf{n}$ from which one direction has to be chosen. We choose the direction of the maximum displacement gradient by maximizing

$$g = \underbrace{max}_{l} \left(\mathbf{n}_l^T \cdot (\nabla \mathbf{u} \cdot \mathbf{h}_l) \right), \quad l = 1, 2 \tag{3}$$

where the normals $\mathbf{n}_l$ correspond to minima of $\mathbf{Q}$, eq. (2). $\mathbf{h}$ is the corresponding eigenvector of $\mathbf{Q}$.

$$F_{ij}|_{\Gamma^c} = \frac{\partial u_i}{\partial X_j} + \delta_{ij} = \lim_{w \mapsto 0} \frac{[[\boldsymbol{u}]]_i}{w n_j} + \delta_{ij} = \delta_{\Gamma^c} [[\boldsymbol{u}]]_i \otimes n_j + \delta_{ij}$$

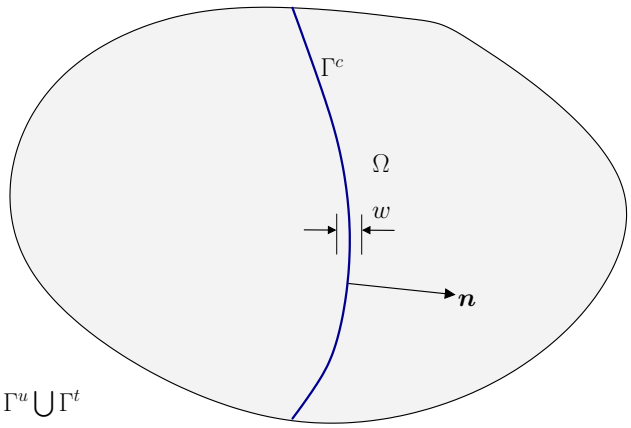

Figure 1. Computation of the discontinuous deformation gradient in the crack surface

3. POST-LOCALIZATION BEHAVIOR

Once the material loses stability, the use of standard governing equations leads to ill-posedness of the IBVP. Several remedies to this problem have been proposed. One of them is to include some dissipative mechanism. The dissipative mechanism replaces the continuum dissipation mechanism in the localized areas. It is possible to have dissipation and maintain hyperbolicity, e.g. if strain hardening occurs and an associated model is employed.

Within the context of nonlinear fracture mechanics, these dissipative mechanisms have been introduced by means of the so-called cohesive surfaces (Dugdale [14], Barenblatt [5]). We adopt a similar methodology here for modelling slip lines, which takes into account the particularities of their kinematical behavior.

3.1. IBVP with an dissipative interface

Consider a solid Ω with material points $\mathbf{X}$. Its boundary Γ is partitioned into three subsets, Γ^t, Γ^u and Γ^c, upon which tractions, displacements and cohesive forces are applied, see figure 1.

We will consider for a given time t the space S_t of suitably smooth functions, i.e. C^0 functions. The set of points having jump discontinuities (the singular set) will be determined by loss of hyperbolicity of the acoustic tensor. Let us also define the corresponding space of test functions as

$$V_t := \{\delta\mathbf{u};\ \ \mathbf{u}_t + \delta\mathbf{u} \in S_t,\ \ \mathbf{u}_t \in S_t \text{ except on } \Gamma^c\} \tag{4}$$

GIVEN the initial displacement, $\mathbf{u}_0$, and the initial stress, $\boldsymbol{\sigma}_0$,

FIND $\mathbf{u}_t \in S_t$ for every time t in the time interval of analysis

SUCH THAT, for all $\delta\mathbf{u} \in V_t$,

$$\int_\Omega \rho\delta\mathbf{u}\cdot\ddot{\mathbf{u}}d\Omega = \int_{\Omega_0\setminus\Gamma_0^c} (\nabla_0 \otimes \delta\mathbf{u}) : \mathbf{P}d\Omega_0 - \int_\Omega \delta\mathbf{u}\cdot\mathbf{b}d\Omega - \int_{\Gamma^t} \delta\mathbf{u}\cdot\mathbf{t}d\Gamma + \int_{\Gamma^c} \delta[\![\mathbf{u}]\!]\cdot\mathbf{t}^c d\Gamma \quad (5)$$

where ρ is the mass density, $\ddot{\mathbf{u}}$ is the acceleration, $\mathbf{b}$ are the body forces, $\mathbf{t}$ is the applied traction, $\mathbf{t}^c$ is the cohesive traction that acts across the slip line and $\mathbf{P}$ is the nominal stress; ∇_0 denotes spatial derivatives with respect to material coordinates. We will also use the updated Lagrangian description where convenient.

3.2. Constitutive model

3.2.1. Continuum model We assume that the constitutive behavior in $\Omega \setminus \Gamma^c$ is governed by a continuum constitutive model, whereas the material description on Γ^c will be ruled by a traction-separation model (often called a cohesive law).

For the continuum model, a Drucker-Prager plasticity model with an isotropic hardening/softening law is considered.

The incremental form of the constitutive model is given by

$$d\boldsymbol{\sigma} = \mathbf{C} : (d\boldsymbol{\epsilon} - d\boldsymbol{\epsilon}^p) \quad (6)$$

where $d\boldsymbol{\epsilon}$ and $d\boldsymbol{\epsilon}^p$ is the total strain increment and plastic strain increment, respectively, $\mathbf{C}$ is the tangent stiffness and $d\boldsymbol{\sigma}$ is the stress increment. For an associated flow rule (the dilation angle is equal to the friction angle), the plastic strain increment is obtained by

$$d\boldsymbol{\epsilon}^p = d\lambda \frac{\partial f}{\partial \boldsymbol{\sigma}} \quad (7)$$

with

$$\begin{aligned} d\lambda &= 0 \ \forall\ f < 0 \text{ or } f = 0 \text{ and } df < 0 \\ d\lambda &> 0 \ \forall\ f = 0 \text{ and } df = 0 \end{aligned} \quad (8)$$

where λ is the plastic multiplier.

A general form of a yield surface with isotropic hardening has the form

$$f(\boldsymbol{\sigma}, \boldsymbol{\epsilon}^p, k) = 0 \quad (9)$$

and the consistency condition has the following format:

$$df = \frac{\partial f}{\partial \boldsymbol{\sigma}} d\boldsymbol{\sigma} + \frac{\partial f}{\partial \boldsymbol{\epsilon}^p} d\boldsymbol{\epsilon}^p + \frac{\partial f}{\partial k} dk = 0 \quad (10)$$

The Drucker-Prager yield surface is

$$f(\boldsymbol{\sigma}, \epsilon^p) = \alpha\ I_1 + \sqrt{J_2} - k(\epsilon_p) = 0 \quad (11)$$

where I_1 is the first invariant of the stress tensor and J_2 is the second invariant of the deviatoric stress tensor. For more details, see e.g. Chen and Han [13].

We would like to mention that in extended versions of the Drucker-Prager model a non-associated flow rule is often used and the dilation angle is usually smaller than the friction angle. If the dilation angle is zero, the inelastic deformations become incompressible.

3.2.2. Interface model The linear cohesive model has the form:

$$\dot{t}_T^c = c[\![\dot{u}]\!]_T \quad \text{on } \Gamma^c \tag{12}$$

where $\dot{t}_T^c$ is the cohesive traction in the shear plane. The constant c can in general be chosen arbitrarily. We have also used exponential cohesive models of the form:

$$t_T^c = t_i e^{(a|[\![\dot{u}]\!]_T|)} \quad \text{on } \Gamma^c \tag{13}$$

where a is constant that is negative and t_i is the initial traction at time of failure. Let $\boldsymbol{e}_T$ denote vector fields on Γ^c orthogonal to $\boldsymbol{n}$. Then, the jump in the velocity $[\![\dot{u}]\!]_T$ is easily obtained by $[\![\dot{u}]\!]_T \equiv [\![\dot{\boldsymbol{u}}]\!] \cdot \boldsymbol{e}_T$.

4. DISCRETIZATION

4.1. The EFG method for slip lines

4.1.1. Approximation of the displacement field The approximation of the displacement field is given by:

$$\mathbf{u}^h(\mathbf{X},t) \quad = \quad \sum_{I\in\mathcal{N}} \Phi_I(\mathbf{X})\ \mathbf{u}_I(t) + \sum_{I\in\mathcal{N}_c} \Phi_I(\mathbf{X})\ S(f_I(\mathbf{X}))\ q_I(t)\ \mathbf{e}_T(\mathbf{X}) \tag{14}$$

where $\mathbf{X}$ is the material coordinate, $\mathbf{u}_I$ are the particle displacements, t is the time, $\Phi_I(\mathbf{X})$ are the shape functions, $\mathcal{N}$ is the total set of nodes in the model and $\mathcal{N}_c$ the set of sheared nodes. Standard EFG shape functions are used that are computed by

$$\Phi_I = \mathbf{p}(\mathbf{X})^T\, \mathbf{A}(\mathbf{X})^{-1}\, \mathbf{D}(\mathbf{X}_J) \tag{15}$$

$$\mathbf{A}(\mathbf{X}) = \sum_J\ \mathbf{p}(\mathbf{X}_J)\, \mathbf{p}^T(\mathbf{X}_J)\, W(\mathbf{X}-\mathbf{X}_J, h) \tag{16}$$

$$\mathbf{D}(\mathbf{X}_J) = \mathbf{p}(\mathbf{X}_J)\, W(\mathbf{X}-\mathbf{X}_J, h) \tag{17}$$

Hereby, $\mathbf{p}$ are the base polynomials, W is the weighting or kernel function, and h is the size of the domain of influence, that is chosen to be 3 times the distance between the particles. The base polynomials are chosen to be $\mathbf{p} = (1, X, Y)$. For more details, see e.g. Belytschko et al. [8], Belytschko and Lu [10], Belytschko et al. [11], Rabczuk et al. [26].

To model the discontinuous part of the displacement, the displacement field is enriched with sign functions which are parameterized by q. Only sheared nodes are enriched. $\mathbf{e}_T(\mathbf{X})$ is the unit vector that spans the plane of the shear band, i.e. $\mathbf{e}_T(\mathbf{X})$ is orthogonal to $\mathbf{n}$. We have chosen the same shape functions Φ_I for the continuous and discontinuous part of the displacements, but this is not mandatory. In contrast to Rabczuk and Belytschko [23, 25], linear and higher order complete basis polynomials are chosen for the EFG shape functions. A more detailed description concerning EFG can be found e.g. in Belytschko and Lu [10], Belytschko et al. [11]. The sign function $S(\xi)$ is defined as:

$$S(\xi) = \begin{cases} 1 & if\ \xi > 0 \\ -1 & if\ \xi < 0 \end{cases} \tag{18}$$

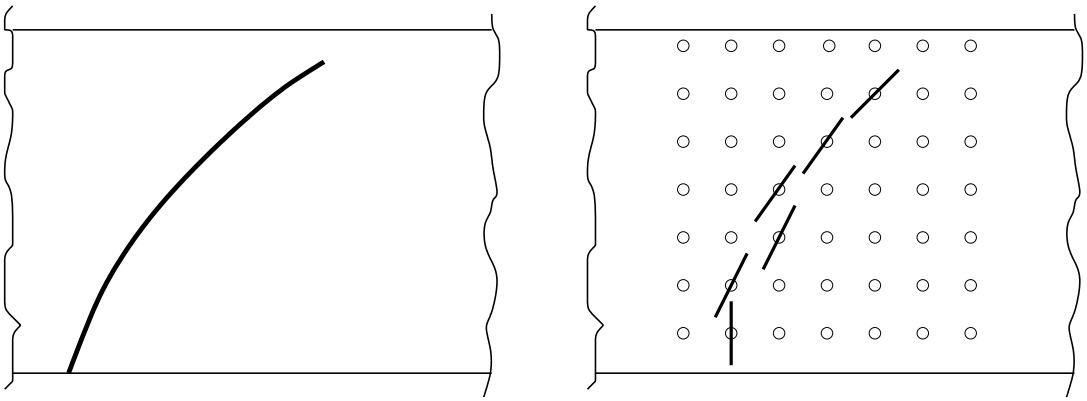

Figure 2. Schematic on the right shows a crack model for the crack on the left

and $f_I(\mathbf{X})$ is given by

$$f_I(\mathbf{X}) = \mathbf{n}_0 \cdot (\mathbf{X} - \mathbf{X}_I) \tag{19}$$

where $\mathbf{n}_0$ is the normal to the crack in the initial configuration. This approach was motivated by the extended finite element method (XFEM), Moes et al. [20]. The principle how to compute the discontinuous deformation gradient is shown in figure 1.

The slip line is modelled by a set of slipped particles as shown in figure 2.

4.1.2. The discrete momentum equation Let us now define the approximation space for the displacement field as

$$\mathcal{V} = \left\{\mathbf{u}(\cdot,t) | \mathbf{u}(\cdot,t) \in H^1 \setminus \Gamma_0^c,\ \mathbf{u}(\cdot,t) \text{ discontinuous on } \Gamma_0^c\,,\ \mathbf{u}(\cdot,t) = \bar{\mathbf{u}}(t) \text{ on } \Gamma_0^u\right\} \tag{20}$$

and for the test functions as

$$\mathcal{V}_0 = \left\{\delta\mathbf{u} | \delta\mathbf{u} \in H^1 \setminus \Gamma_0^c,\ \delta\mathbf{u} \text{ discontinuous on } \Gamma_0^c\,,\ \delta\mathbf{u} = 0 \text{ on } \Gamma_0^u\right\} \tag{21}$$

After substituting the approximations of the test and trial functions into eq. (5) we obtain

$$\begin{aligned} &\sum_{I\in\mathcal{N}} \delta\mathbf{u}_I \cdot \left(\mathbf{f}_I^{int} + \mathbf{M}_{IK}^{uu} \cdot \ddot{\mathbf{u}}_K + \mathbf{M}_{IK}^{uq}\ \ddot{q}_K - \mathbf{f}_I^{ext}\right) + \\ &\sum_{I\in\mathcal{N}_c} \delta q_I\ \left(Q_I^{int} + \mathbf{M}_{IK}^{uq} \cdot \ddot{\mathbf{u}}_K + \mathbf{M}_{IK}^{qq}\ \ddot{q}_K - Q_I^{ext}\right) = 0 \end{aligned} \tag{22}$$

where

$$\begin{aligned} \mathbf{f}_I^{int} &= \int_{\Omega\setminus\Gamma^c} \nabla\Phi_I(\mathbf{X}) \cdot (\boldsymbol{\sigma}(\mathbf{X}))\ d\Omega \\ \mathbf{f}_I^{ext} &= \int_{\Omega\setminus\Gamma^c} \varrho\mathbf{b}\ \Phi_I(\mathbf{X})\ d\Omega^+ \int_{\Gamma^t} \bar{\mathbf{t}}\ \Phi_I(\mathbf{X})\ d\Gamma \end{aligned} \tag{23}$$

$$
\begin{aligned}
Q_I^{int} &= \int_{\Omega\setminus\Gamma^c} \left(\nabla\Phi_I(\mathbf{X})\otimes\mathbf{e}_T\right)^S : (\boldsymbol{\sigma}(\mathbf{X}))\; d\Omega + \underbrace{\int_{\Omega\setminus\Gamma^c} \Phi_I(\mathbf{X})\left(\nabla\otimes\mathbf{e}_T\right)^S : (\boldsymbol{\sigma}(\mathbf{X}))\; d\Omega}_{=0} \\
Q_I^{ext} &= \int_{\Omega\setminus\Gamma^c} \varrho\,(\mathbf{b}\cdot\mathbf{e}_T)\;\Phi_I(\mathbf{X})\; d\Omega^+ \int_{\Gamma^t} (\bar{\mathbf{t}}\cdot\mathbf{e}_T)\;\Phi_I(\mathbf{X})\; d\Gamma - \int_{\Gamma^c} \mathbf{t}^c\Phi_I(\mathbf{X})\;[\![S(f_I(\mathbf{X}))]\!]
\end{aligned}
\tag{24}
$$

where the spatial derivatives with respect to $\mathbf{e}_T$ vanish since the discontinuity is piecewise constant. Note that if the crack is modeled continuous, no curvature of the shear band can be captured if this term is dropped.

The mass matrix is

$$
\mathbf{M}_{IJ} = \begin{bmatrix} \mathbf{m}_{IJ}^{uu} & \mathbf{m}_{IJ}^{uq} \\ \mathbf{m}_{IJ}^{uq} & \mathbf{m}_{IJ}^{qq} \end{bmatrix} \tag{25}
$$

with

$$
\begin{aligned}
\mathbf{m}_{IJ}^{uu} &= \int_{\Omega\setminus\Gamma^c} \varrho_0\;\Phi_I(\mathbf{X})\;\hat{\Phi}_J(\mathbf{X})\;\mathbf{I}\; d\Omega \\
\mathbf{m}_{IJ}^{uq} &= \int_{\Omega\setminus\Gamma^c} \varrho_0\;\Phi_I(\mathbf{X})\;\Phi_J(\mathbf{X})\;S(f_J(\mathbf{X}))\;\mathbf{e}_T\; d\Omega \\
\mathbf{m}_{IJ}^{qq} &= \int_{\Omega\setminus\Gamma^c} \varrho_0\;\Phi_I(\mathbf{X})\;S(f_I(\mathbf{X}))\;\Phi_J(\mathbf{X})\;S(f_J(\mathbf{X}))\; d\Omega \\
&= \int_{\Omega\setminus\Gamma^c} \varrho_0\;\Phi_I(\mathbf{X})\;\Phi_J(\mathbf{X})\; d\Omega
\end{aligned}
\tag{26}
$$

The integrals are evaluated by a stress-point integration, see e.g Rabczuk and Belytschko [23].

5. EXAMPLES

5.1. Sand under biaxial compression

Consider a sand specimen under biaxial loading condition. The dimensions of the problem are shown in figure 3. The specimen is fixed at the right hand side and a slow displacement boundary condition is applied on the left hand side. The lateral confinement is 0.2 MPa. There exists a variety of experimental data of above described tests. Vardoulakis et al. [31] performed a series of different sand specimen, different in the sense that the sand was pre-consolidated or had different grain size, etc. Han and Drescher [17] give results for dry Ottawa sand. Numerical results are also available, see e.g. Anand and Gu [2]. A common slip line pattern in the above mentioned experiments is shown in figure 3. The shear band slopes ranged from 52 to 65 degree against the vertical axis. Han and Drescher [17] was able to reproduce the load deflection curve and the slope of the shear band of 56 degree from their experiments very well. We will use this model to verify our method. However, our intention is to show the applicability of our method rather than the exact reproduction of the experiments since the Drucker-Prager model is not established for this kind of problem.

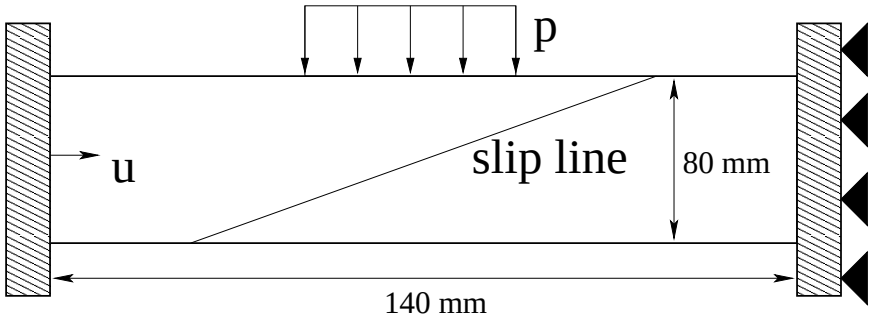

Figure 3. Test setup of the sand specimen under biaxial compression load

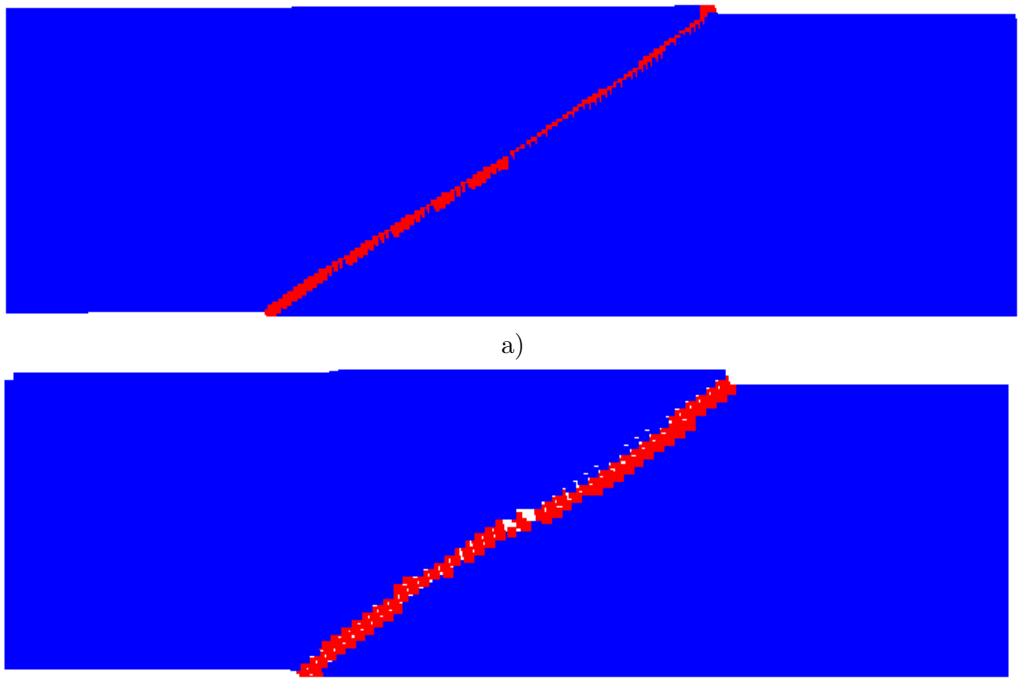

a)

b)

Figure 4. Slip line of the sand under biaxial compression for a) 16,000 particles, b) 4000 particles;

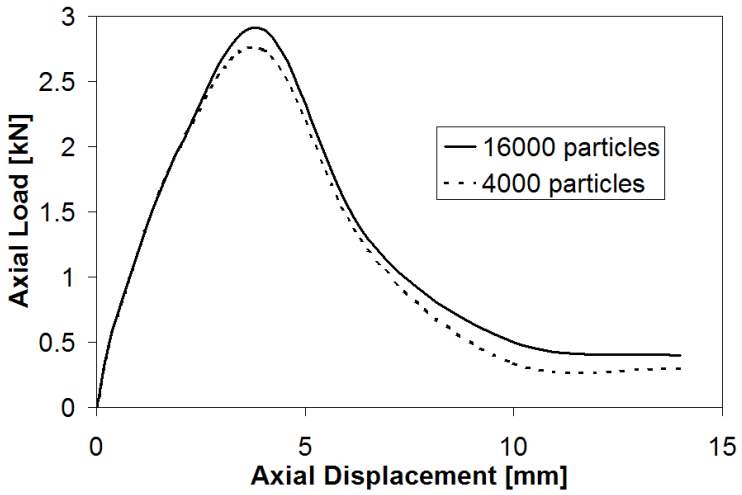

Figure 5. Load deflection curve of the sand under biaxial compression for different numbers of particles

We used two different refinements, 16000 and 4000 particles. The Young's modulus is $200,000$ MPa, Poisson ratio $\nu = 0.1$ and density 0.002 g/mm^3. Particles in the middle of the specimen are attributed a smaller density. An exponential decaying cohesive model was applied with a "fracture energy" of $G_f = 1500$ J/m^2. We tested different friction angles from 30 to 40 degree. We also tested the influence of associated and non associated flow rule where we only considered the extreme case of a dilation angle of 0 degree. As expected, by increasing the friction and dilation angle the slip line becomes steeper (the slip line angle becomes larger) though the results do not differ much (maximum of 9 degree). A typical slip line pattern for two particle discretizations is shown in figure 4a,b. The slip line is sloped with an 56 degree angle against the vertical axis which lies in the experimental data from Han and Drescher [17] or Vardoulakis et al. [31]. The load deflection curve for this example is shown in figure 5. The results are reproduced mesh independent.

5.2. Excavation problem

Consider the plain strain excavation problem as shown in figure 6. A similar example was used by Regueiro and Borja [27] to demonstrate the power of the embedded element method. They used a non-associated Drucker-Prager model in the continuum region. The boundary conditions and the excavation steps are shown in figure 6. Gravity load is applied. The soil is removed on the left hand side according to figure 6. This example shows the applicability of the method to large deformations. We made up the material parameters so that we obtained a nice landslide. One difficulty when modelling soil is the identification of material parameters. We used 10,000 and 40,000 particles for this simulation. The slip line and the corresponding effective plastic strain is shown in figure 7. As can be seen, plastic deformation occur before a slip line develops. The results do not show discretization dependence.

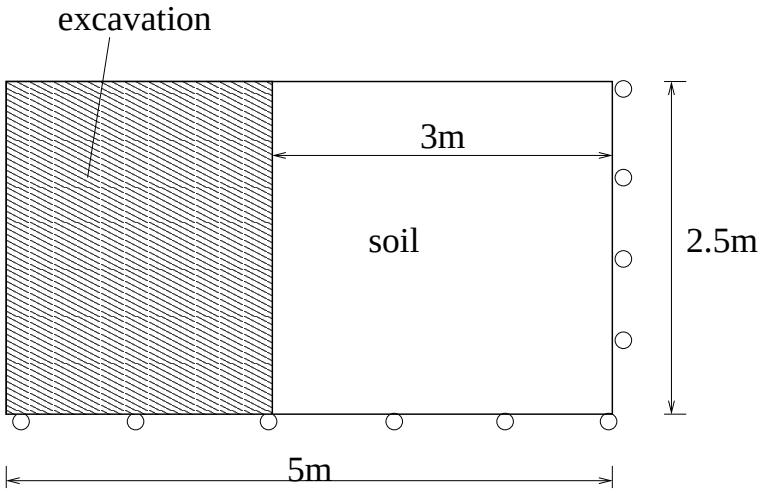

Figure 6. Excavation problem

5.3. Inflation of a cavity in a thick-walled cylinder

Alsiny et al. [1] performed experiments on sand filled thick-walled cylinders under external pressure. The test-setup is shown in figure 8. The inner diameter of the cylinder is 30 mm and the outer diameter is 300 mm. They reported curved slip lines that cross the entire specimen. They used the same coarse Ottawa sand as in Han and Drescher [17]. Hence, the material parameters are the same as in section 5.1. The computational slip line pattern is shown in figure 9. We are able to capture the experimental slip line pattern. This example shows also the ability of our method for multiple slip-lining with intersections.

6. CONCLUSIONS AND FUTURE WORK

We have presented a meshfree method for modelling slip lines with cohesive surfaces in meshfree methods. The slip line is modelled by a set of slipped particles at each of which a discontinuity jump in the tangential direction of the displacement is introduced. Loss of hyperbolicity was used as slip line initiation criterion. The introduction of cohesive surfaces removes the necessity of regularization techniques. For sake of simplicity, we used the Drucker-Prager model though more complicated constitutive models can be used.

We have applied the method to several two-dimensional problems though the method can readily be used in three dimensions. We showed that experimental results can qualitatively be reproduced and that the results are mesh independent. For two problems, the performance of the method regarding the initiation and propagation of multiple slip lines including branching was shown. Branching occurs naturally. No special criteria have to be introduced to predict branching.

One difficulty occurs at slip line intersection. At slip line intersections, the propagating slip

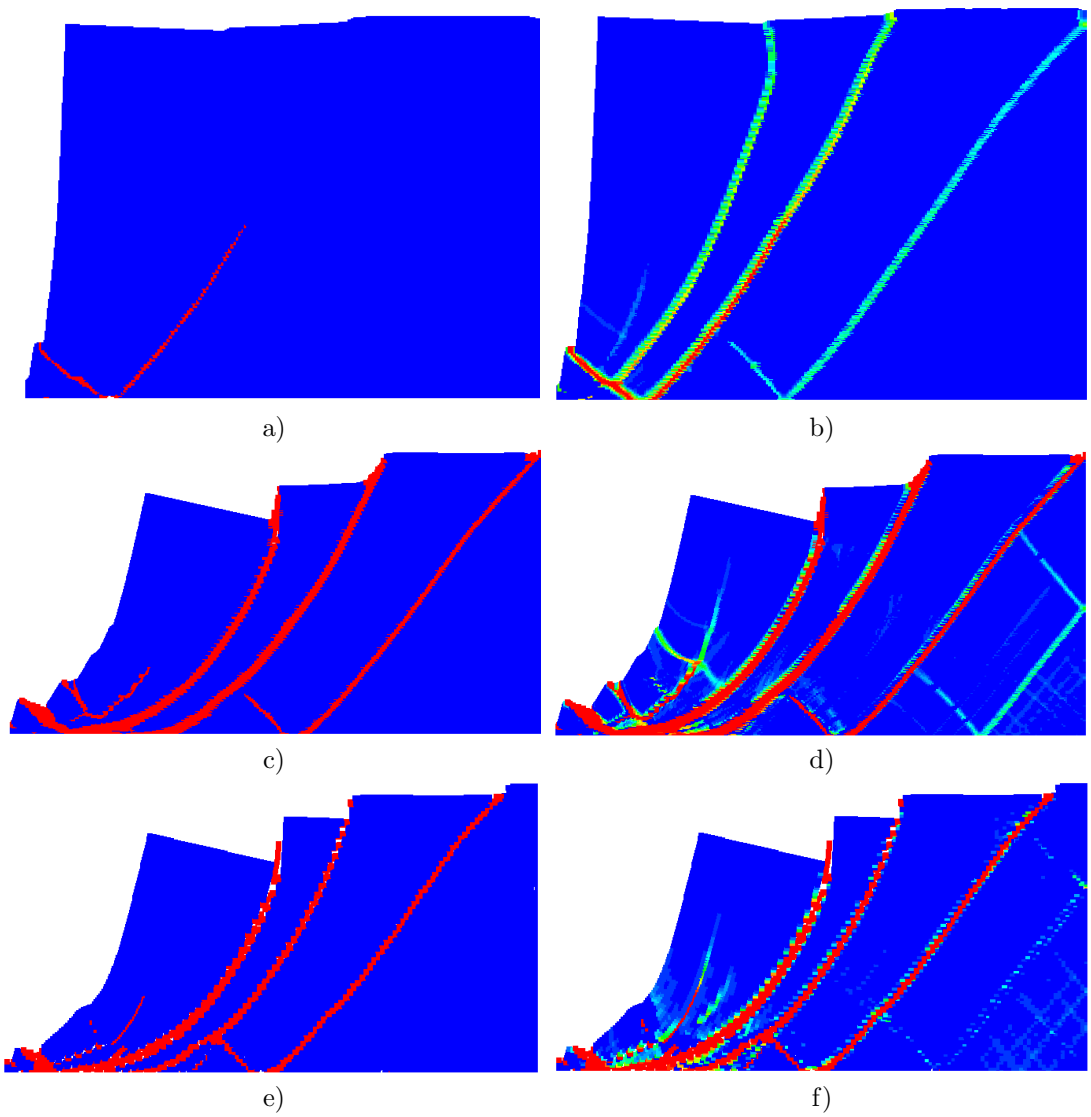

Figure 7. For the 40,000 particle discretization: a),c) slip line, b),d) effective plastic strain; for the 10,000 particle discretization: e) slip line, f) effective plastic strain

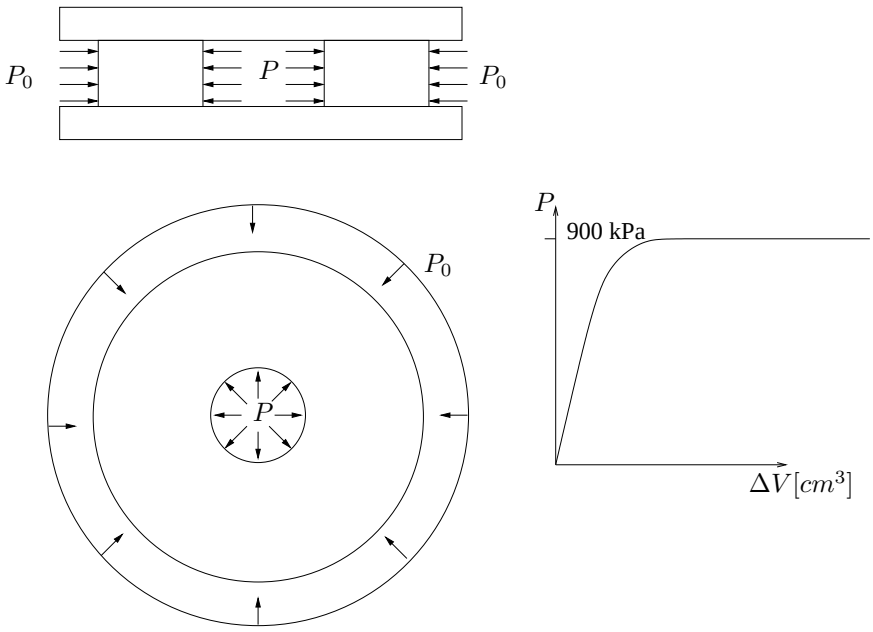

Figure 8. Test-setup of the cavity inflation problem of a thick walled cylinder

line tends to stop when it hits the intersection. Loss of hyperbolicity cannot be checked at the intersection points since the PDE already lost hyperbolicity. Therefore, the direction of the slip line of the slipped particles at the intersection points are rotated into the proper (=the direction of the crossing shear band) position to allow the slip line to propagate.

In future, more sophisticated continuum models can be employed that allow better quantitative predictions. To obtain better accuracy around the slip line tip, adaptive methods can be used. Meshfree methods are ideally suited since h-adaptivity can easily be incorporated. This was already exploited for crack and shear band problems, [24, 25] and improved the accuracy of the method and decreased the computational cost as well.

7. ACKNOWLEDGEMENT

The support of Office of the Naval Research and the Army Research Office is gratefully acknowledged.

references

[1] A. Alsiny, I. Vardoulakis, and A. Drescher. Deformation localization in cavity inflation experiments on dry sand. *Geotechnique*, 42:395–410, 1992.

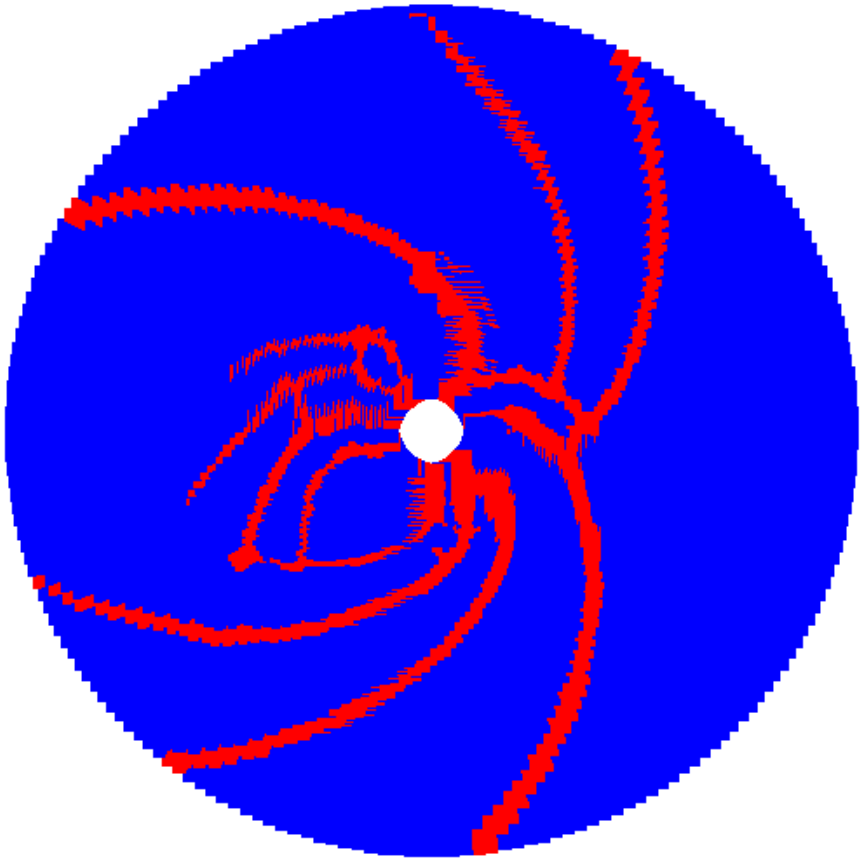

Figure 9. Slip line pattern of the cavity inflation problem

[2] L. Anand and C. Gu. Granular materials: constitutive equations and strain localization. *Journal of the Mechanics and Physics of Solids*, 48:1701–1733, 2000.

[3] P.M.A. Areias and T. Belytschko. Two scale shear band evolution with adaptive bandwidth by local partition of unity. *International Journal for Numerical Methods in Engineering*, in Press.

[4] F. Armero and K. Garikipati. An analysis of strong discontinuities in multiplicative finite strain plasticity and their relation with the numerical simulation of strain localization in solids. *International Journal of Solids and Structures*, 33(20-22):2863–2885, 1996.

[5] G. Barenblatt. The mathematical theory of equilibrium of cracks in brittle fracture. *Advances in Applied Fracture*, 7:55–129, 1962.

[6] T. Belytschko, H. Chen, J. Xu, and G. Zi. Dynamic crack propagation based on loss of

hyperbolicity and a new discontinuous enrichment. *International Journal for Numerical Methods in Engineering*, 58(12):1873–1905, 2003.

[7] T. Belytschko, J. Fish, and B. Englemann. A finite element method with embedded localization zones. *Computer Methods in Applied Mechanics and Engineering*, 70:59–89, 1988.

[8] T. Belytschko, Y. Krongauz, D. Organ, M. Fleming, and P. Krysl. Meshless methods: An overview and recent developments. *Computer Methods in Applied Mechanics and Engineering*, 139:3–47, 1996.

[9] T. Belytschko, W. K. Liu, and B. Moran. *Nonlinear Finite Elements for Continua and Structures*. John Wiley and Sons, Chichester, 2000.

[10] T. Belytschko and Y.Y. Lu. Element-free galerkin methods for static and dynamic fracture. *International Journal of Solids and Structures*, 32:2547–2570, 1995.

[11] T. Belytschko, Y.Y. Lu, and L. Gu. Element-free galerkin methods. *International Journal for Numerical Methods in Engineering*, 37:229–256, 1994.

[12] G. T. Camacho and M. Ortiz. Computational modeling of impact damage in brittle materials. *International Journal of Solids and Structures*, 33:2899–2938, 1996.

[13] W. Chen and D. Han. *Plasticity for Structural engineers*. Springer-Verlag, 1988.

[14] D. Dugdale. Yielding of steel sheets containing slits. *Journal of the Mechanics and Physics of Solids*, 8:100–108, 1960.

[15] M.L. Falk, A. Needleman, and J.R. Rice. A critical evaluation of cohesive zone models of dynamic fracture. *Journal of Physics IV 11 (PR5)*, pages 43–50, 2001.

[16] A. Gravouil, N. Moes, and T. Belytschko. Non-planar 3D crack growth by the extended finite element and level sets - part ii: Level set update. *International Journal for Numerical Methods in Engineering*, 53:2569–2586, 2002.

[17] C. Han and A. Drescher. Shear bands in biaxial tests on dry coarse sand. *Soils and Foundations*, pages 118–132, 1993.

[18] J. E. Marsden and T.J.R Hughes. *Mathematical Foundations of Elasticity*. Dover Publications Inc., New York, 1983.

[19] N Moes and T. Belytschko. Extended finite element method for cohesive crack growth. *Engineering Fracture Mechanics*, 69:813–834, 2002.

[20] N. Moes, J. Dolbow, and T. Belytschko. A finite element method for crack growth without remeshing. *International Journal for Numerical Methods in Engineering*, 46(1):133–150, 1999.

[21] J. Oliver, M. Cervera, and O. Manzoli. Strong discontinuities and continuum plasticity models: the strong discontinuity approach. *International Journal of Plasticity*, 15:319–351, 1999.

[22] M. Ortiz, Y. Leroy, and A. Needleman. Finite element method for localized failure analysis. *Computer Methods in Applied Mechanics and Engineering*, 61(2):189–214, 1987.

[23] T. Rabczuk and T. Belytschko. Cracking particles: A simplified meshfree method for arbitrary evolving cracks. *International Journal for Numerical Methods in Engineering*, 61(13):2316–2343, 2004.

[24] T. Rabczuk and T. Belytschko. Adaptivity for structured meshfree particle methods in 2D and 3D. *International Journal for Numerical Methods in Engineering*, 63(11):1559–1582, 2005.

[25] T. Rabczuk and T. Belytschko. A three dimensional large deformation meshfree method for arbitrary evolving cracks. *Computer Methods in Applied Mechanics and Engineering*, in progress.

[26] T. Rabczuk, T. Belytschko, and S.P. Xiao. Stable particle methods based on lagrangian kernels. *Computer Methods in Applied Mechanics and Engineering*, 193:1035–1063, 2004.

[27] R.A. Regueiro and R.I. Borja. Finite element analysis of strain localization in geologic materials taking a strong discontinuity approach. *John A. Blume Earthquakt Engineering Center*, 14, 1998.

[28] E. Samaniego and T. Belytschko. Continuum-discontinuum modelling of shear bands. *International Journal for Numerical Methods in Engineering*, 62:1857–1872, 2005.

[29] M. Silhavy. *The Mechanics and Thermodinamics of continuous media*. Springer Verlag, Berlin, 1997.

[30] J. C. Simo, J. Oliver, and F. Armero. An analysis of strong discontinuities induced by strain-softening in rate-independent inelastic solids. *Computational Mechanics*, 12:277–296, 1993.

[31] I. Vardoulakis, M. Goldscheider, and G. Gudehus. Formation of shear bands in sand bodies as a bifurcation problem. *International Journal for numerical and analytical methods in geomechanics*, 2:99–128, 1978.

[32] G. Ventura, B. Moran, and T. Belytschko. Dislocations by partition of unity. *International Journal for Numerical Methods in Engineering*, 62(11):1463–1487, 2005.

[33] X.-P. Xu and A. Needleman. Numerical simulations of fast crack growth in brittle solids. *Journal of the Mechanics and Physics of Solids*, 42:1397–1434, 1994.

[34] Q. Yang, A. Mota, and M. Ortiz. A class of variational strain-localization finite elements. *International Journal for Numerical Methods in Engineering*, 62(8):1013–1037, 2005.

[35] F. Zhou and J.F. Molinari. Dynamic crack propagation with cohesive elements: a methodolgy to address mesh dependence. *International Journal for Numerical Methods in Engineering*, 59(1):1–24, 2004.